Modelling and Verification of Nonlinear Electromechanical Coupling in Micro-Scale Kinetic Electromagnetic Energy Harvesters

Andrii Sokolov[ID], *Student Member, IEEE*, Dhiman Mallick[ID], *Member, IEEE*, Saibal Roy[ID], Michael Peter Kennedy[ID], *Fellow, IEEE*, and Elena Blokhina[ID], *Senior Member, IEEE*

Abstract—**Electromechanical coupling in kinetic energy harvesters is the key aspect of these devices that ensures an effective energy conversion process. When modelling and designing such devices, it is necessary to incorporate electromechanical coupling correctly since it will determine the amount of energy that will be converted during its operation. As the engineering community prefers compact (lumped) models of such devices, the conventional choice of the lumped model for the electromagnetic type of electromechanical coupling is linear damping, proportional to the velocity of the mechanical resonator in a harvester, leading to the idea of maximizing the velocity in order to improve the energy conversion process. In this paper, we show that electromechanical coupling in electromagnetic kinetic energy harvesters is inherently nonlinear and requires a number of aspects to be taken into account if one wants to optimize a device. We show that the proposed model, which is based on first principles of electromagnetics, can be reduced to a nonlinear lumped model that is particularly convenient for analysis and design. The modelling approach and the resulting lumped model are verified using two MEMS electromagnetic harvesters operating over a range of frequencies from 300 to 500 Hz (Harvester A) and from 50 to 70 Hz (Harvester B) generating from mV (Harvester A) to few volts (Harvester B) of RMS voltage, respectively. The proposed modelling approach is not limited to energy harvesters but can also be applied to magnetic sensors or other MEMS devices that utilise electromagnetic transduction.**

Index Terms—**MEMS interface, electromagnetic transduction, MEMS kinetic energy harvesting, lumped modelling, numerical methods, modelling and simulations, mixed-domain modelling, computer aided design.**

I. Introduction

KINETIC energy harvesting is a technique to convert the motion of the environment to electricity. It has been

Fig. 1. (a) Schematic block diagram of a typical kinetic (vibration) energy harvester utilizing the electromagnetic transduction mechanism. The following convention will be used: displacement z and velocity u_z (belong to the mechanical domain) and current i and voltage v (belong to the electrical domain). The electromagnetic force F_{EM} provides transduction between the mechanical and electrical domains. The magnetic proof-mass oscillates in the vicinity of a coil. As a 3D system, the oscillations of the proof-mass can be classified as (b) translational or (c) rotational.

widely discussed over recent years [1]–[4] with many implementations fabricated using micro- and nano-technologies (NEMS/MEMS). The conventional point of view is that out of three very common transduction mechanisms, the piezoelectric and electrostatic ones are particularity compatible with MEMS while the electromagnetic mechanism is seen as inefficient at a micro-scale. However, since the first implementations reported in the literature [5], many configurations of electromagnetic kinetic energy harvesters (emKEH) have been reported [6]–[14]. Electromagnetic harvesters show effectiveness similar to that of piezoelectric and electrostatic harvesters and feature nonlinear behaviour that allows them to increase the converted power and frequency band. An example of an emKEH is shown in Fig. 1(a) illustrating the electromagnetic transduction. A linear or nonlinear micromechanical resonator, with a magnet attached to it, moves as a response to external vibrations provided by the environment. The moving magnet creates a variable magnetic flux through a (usually) fixed coil

that is placed in the vicinity of the magnet. By Faraday's law, this induces a voltage in the coil, and if a resistor is connected to the coil, the power converted from the mechanical to the electrical domain will be dissipated in the resistor.

The design, analysis and characterisation of a kinetic energy harvester (KEH) can be a challenging task for a number of reasons. Firstly, a KEH is a device combining at least two physical domains (mechanical and electrical) and a specific device may have a particularly advanced mechanical configuration with translational and rotational motion induced by ambient vibrations. Secondly, only the electrical response (voltage v and current i) of a device is usually observed and measured upon the application of external stimuli. In many cases, it is difficult or even impossible to access the mechanical state (displacement z and velocity $u_z = \dot{z}$) of a device. In addition to the above, the three common transduction mechanisms—piezoelectric, electrostatic and electromagnetic—that are responsible for electromechanical coupling are nonlinear in the most general case. For these reasons, the extraction of device parameters from an experiment and optimisation of a device become quite difficult.

With regard to emKEHs, while first principles of Electromagnetics are well understood, their application to a particular device usually results in equations written in three-dimensions. Since the research community prefers simplified lumped models, it is very common to see linear equations describing the electromagnetic mechanism in emKEHs. Usually, the electromotive force (e.m.f.) that expresses electromechanical coupling in the electrical domain is written as $B\,l\,\dot{z}$. On the other hand, the magnetic force that expresses electromechanical coupling in the mechanical domain is written as $B\,l\,i$. It is said that B is the magnitude of the magnetic field (in the form of the magnetic flux density) generated by the magnet and l is the length of the coil [15]–[18]. This simplification is not valid for typical emKEH configurations as we will show.

The aim of this paper is to develop a modelling framework allowing one to obtain nonlinear lumped models of the electromagnetic type of electromechanical coupling. We begin with the equations summarising the first principles of Mechanics and Electromagnetics, arriving to a model that uses only the physical parameters of the device. The resulting model is lumped, i.e., it utilises a finite number of electrical and mechanical variables. We address the issue of model self-consistency which is often overlooked in such examples of mixed-domain modelling and simulations. The proposed model is not limited to energy harvesters but can be applied to magnetic sensors or other MEMS devices utilising electromagnetic transduction.

Compared to the conference paper which introduced the approach described in this work [19], the presented manuscript contains the following new features. In addition to the detailed analysis of translational motion, we also present a compact model of rotational motion that, to the knowledge of the authors, has never been derived in the literature for such systems. The model describing rotational motion is also lumped and follows the same methodology as that for the translational mode. For both translational and rotational modes, we show how to calculate shape functions to obtain self-consistent lumped models of the generated electromotive and electromagnetic force. We use two examples of the most recent MEMS implementation of emKEHs of very different topologies to validate the methodology. The design of the experiments, data collection and data analysis are original to this manuscript and have not been presented elsewhere.

The paper is organised as follows. Section II presents the fundamental equations describing an emKEH in the mechanical and electrical domains. The presented statement of the problem is original, and, to the knowledge of the authors of this paper, has not been presented previously in the literature. Since the mechanical resonator of a KEH is a three-dimensional structure, it can exhibit spatial eigen-modes of different types, translational and rotational, and both types are taken into account in the statement of the problem. The statement of the problem also shows that the underlying quantity required to complete the model is the magnetic flux density. Section III presents different techniques to calculate the magnetic flux density. Despite the fact that it is a three-dimensional vector field, there are simple and effective techniques to calculate it. Section IV demonstrates a technique to reduce the model to a lumped one using shape functions. These functions are calculated for translational and rotational modes. They characterise the geometry of the system and do not depend on the mechanical parameters of the MEMS resonator. Section V explains the design of the experiment to validate the proposed model. Finally, Section VI presents the measured data and compares the results of experiments and modelling carried out for two devices with different configurations.

II. STATEMENT OF THE PROBLEM

We begin by presenting a self-consistent model of a harvester that will take into account the dynamics of its resonator (a magnetic proof-mass suspended on springs) in the mechanical domain, the coupling between the mechanical and electrical domains and the harvester state in the electrical domain. The formulated model will be valid for both types of oscillation modes of the mechanical resonator, translational and rotation, as well as their combination. The model presented in this Section will be the primary object of investigation and experimental validation in the paper. To the knowledge of the authors, this statement of the problem, while it is based on general principles, is original and has not been proposed or developed in the literature, in particular, for rotational type of motion.

A. Self-Consistent Dynamical Model of emKEH Including the Mechanical and Electrical Components

As a distributed mechanical system, the resonator (a magnetic proof-mass supported by springs) of a harvester can display different types of oscillations associated with spatial eigen-modes. The actuation of different modes depends primarily on the frequency of the actuating force [20], [21]. They are often classified into translational and rotational modes. Schematic views of these modes are shown in Fig. 1(b) and Fig. 1(c) respectively. When building a lumped model, one

This article has been accepted for inclusion in a future issue of this journal. Content is final as presented, with the exception of pagination.

SOKOLOV *et al.*: MODELLING AND VERIFICATION OF NONLINEAR ELECTROMECHANICAL COUPLING

3

follows a very common approach and reduces the partial differential equation describing a distributed system to an ordinary differential equation, i.e., a lumped model. There are many methods allowing such a reduction (see, for instance, [22], [23]) to be applied successfully to linear and nonlinear MEMS devices [24], [25].

We will not show the intermediate steps of reduction in this paper, but rather start with the already well-known second-order ordinary differential equation, often referred to as the 'mass-spring-damper' equation, describing the displacement of the resonator from Fig. 1 in the translational mode of oscillations:

$$m\ddot{z}+c_a\dot{z}+kz+F_{nonlin}(z) + F_{EM}(z,\dot{z},i,v)=mA_{ext}\cos(\omega_{ext}t). \quad (1)$$

Here m is the mass of the resonator, z is its displacement, c_a is the linear air damping (dissipation) coefficient, k is the linear spring constant, $F_{nonlin}(z) = \sum_{j=2}^{N} k_j z^j$ is the nonlinear restoring force, A_{ext} and ω_{ext} are the magnitude of the external acceleration and the cyclic frequency of the external vibrations driving the harvester, respectively. We use polynomial of order up to $N = 5$ to describe the nonlinearity of the restoring forces in the harvesters presented in the paper for validation. The magnetic force $F_{EM}(z,\dot{z},i,v)$ depends on both the electrical and mechanical states of the system through the displacement z, the velocity $u_z = \dot{z}$, the current i and voltage v, and, hence, relates both domains. The presence of mechanical $F_{nonlin}(z)$ and electrical nonlinearities is very common in MEMS resonators [3], [21], [26], [27].

A similar formula is used to describe rotational motion of the proof-mass, but the angle of rotation φ is used instead of the linear displacement z. It can be shown that equation (1) can be transformed into the following expression [20]:

$$I\ddot{\varphi} + c_a'\dot{\varphi} + k'\varphi + M_{nonlin}(\varphi) + M_{EM}(\varphi,\dot{\varphi},i,v)$$
$$= I\varepsilon_{ext}\cos(\omega_{ext}t). \quad (2)$$

Here I is the moment of inertia of the proof-mass, φ is its rotation angle, $\omega = \dot{\varphi}$ is the angular velocity, c' is the analogue of the air dissipation coefficient for the rotational mode, k' is the analogue of the spring coefficient, $M_{nonlin}(\varphi)$ is the nonlinear restoring moment, M_{EM} is the analogue of the electromagnetic force in translational mode, the magnetic torque acting of the proof-mass, ε_{ext} is the amplitude of the external angular acceleration applied to the device, which is linearly proportional to the translational acceleration A_{ext}.

The state in the harvester must also be represented in the electrical domain, see again Fig. 1(a). For both translational and rotational modes we use the Kirchhoff Voltage Law (KVL):

$$L\frac{di}{dt} + R_{load}i - \mathcal{E} = 0, \quad (3)$$

where i is the current flowing in the loop obtained when the coil is connected to a load resistor, L is the inductance of the coil, R_{load} is the total resistance of the coil and the load resistor and $\mathcal{E}$ is the e.m.f. induced in the coil. The e.m.f. is
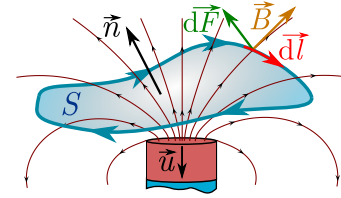

Fig. 2. Schematic diagram illustrating the origin of the net electromagnetic force $d\vec{F}$ acting on an incremental segment $d\vec{l}$ of a loop with current i placed in a magnetic field $\vec{B}(x,y,z)$. The net force appears when all $d\vec{F}$ are integrated.

related to the total magnetic flux Φ_i passing through the coil loops through Faraday's law of induction:

$$\mathcal{E} = \sum_i \frac{d\Phi_i}{dt}, \quad (4)$$

where the further representation of the derivative of flux with respect to time can be made for the translational mode:

$$\frac{d\Phi_i(z)}{dt} = \frac{d\Phi_i(z)}{dz} \cdot \frac{dz}{dt} = \frac{d\Phi_i(z)}{dz} \cdot \dot{z}, \quad (5)$$

and for the rotational mode:

$$\frac{d\Phi_i(\varphi)}{dt} = \frac{d\Phi_i(\varphi)}{d\varphi} \cdot \frac{d\varphi}{dt} = \frac{d\Phi_i(\varphi)}{d\varphi} \cdot \dot{\varphi}. \quad (6)$$

The complete model is obtained when the magnetic force F_{EM} (or magnetic torque M_{EM} in case of rotation) and the magnetic flux $\Phi(z)$ (or $\Phi(\varphi)$ in case of rotation) are specified from first principles for a particular emKEH configuration.

In the most general case, the magnetic flux Φ depends on the three-dimensional magnetic field (also known as the magnetic induction or magnetic flux density) $\vec{B}(x,y,z)$ generated by a permanent magnet [28]:

$$\Phi_i(z) = \iint (\vec{B} \cdot \vec{n})dS = \iint B_n dS, \quad (7)$$

where $\vec{n}$ is the normal unit vector perpendicular to the surface element S.

The electromagnetic force F_{EM} and torque M_{EM}, as shown in Fig. 2, also depend on $\vec{B}$. In the case of translational motion, for the force F_{EM} used in eq. (1), we write:

$$\vec{F}_{EM} = \oint_{loop} i\left[\vec{B} \times d\vec{l}\right], \quad (8)$$

where $d\vec{l}$ is the infinitesimal displacement vector along the loop of integration. In the case of the rotational mode, for the torque M_{EM} from eq. (2) acting on the magnet, we have:

$$M_{EM} = l \cdot \left|\oint_{loop} i\left[\vec{B} \times d\vec{l}\right]\right|, \quad (9)$$

where l is the projection of the position vector of the proof-mass on the rotation axis. In the most general case, the torque, the rotation angle and the angular velocity are vector quantities. However, in our case the rotation of the proof-mass occurs about a single axis. For this reason, the model developed in this Section utilizes their scalar equivalents.

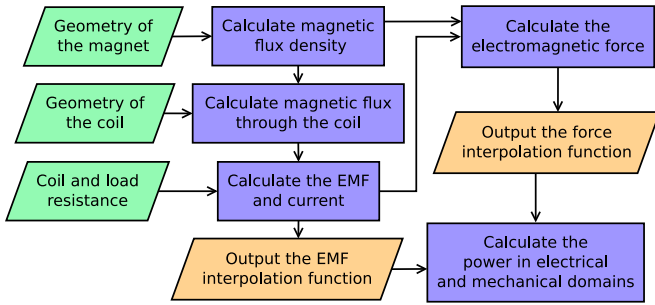Hence, we conclude that the calculation of $\vec{B}(x,y,z)$ generated by an emKEH in three dimensions is the key step

Fig. 3.   The algorithm for calculating the electromagnetic force acting on a coil moving in the magnetic field of a permanent magnet.
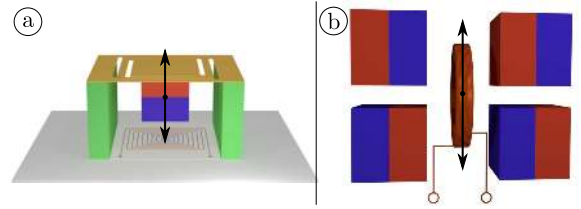

Fig. 4.   Two different devices used to verify our method. (a) MEMS Harvester A with a flat coil and a single permanent magnet oscillator. (b) MEMS Harvester B with an array of permanent magnets and a movable coil.

TABLE I

KNOWN PHYSICAL PARAMETERS OF THE HARVESTER USED
AS A UNIVERSAL EXAMPLE (HARVESTER A)

Parameter	Value
Resonators mass	9.83×10^{-5} kg
Magnet dimensions	$2.5 \times 2.5 \times 2.0$ mm^3
Magnetization	7.6×10^5 A/m
Wire loop dimensions	2.8×2.8 mm^2
Number of loops in the coil	144
Resistance of the coil	192 Ω
Magnet relative speed for the testing problem	0.5 m/s
Wire loop resistance for the testing problem	10.0 Ω

required to complete the model. Knowing $\vec{B}$, we can calculate Φ, the e.m.f. $\mathcal{E}$ and the current i generated in the loop when a load resistor R_{load} is connected to it. We usually assume that the inductance of the loop itself is negligible, and so the current can be found from Ohm's law $i = \mathcal{E}/R_{\text{load}}$. (For this reason, there is no need to use both electrical variables, i and v in the notation and we will omit one of them.) Knowing the flux density $\vec{B}$, we can also calculate the force acting on the coil.

So far, the model is self-consistent and couples the electrical and mechanical domains, but it is not lumped since we are required to know the 3D vector field $\vec{B}$. In order to provide a lumped model, one must obtain expressions for the electromagnetic force $F_{\text{EM}} = F_{\text{EM}}(z, \dot{z}, i)$ and the e.m.f. $\mathcal{E} = \mathcal{E}(z, \dot{z}, i)$ in terms of the lumped variables z, $\dot{z}$ and i. These expressions could be found as an interpolation of the data calculated using the algorithm described in Fig. 3 [19]. Hence, our next step is the analysis of the calculated data sets to identify shape functions and physical parameters for the lumped model of electromagnetic coupling. For illustration purposes throughout the next sections, we will choose some fixed physical parameters for modelling and simulations of the system. They are presented in Table I, and they correspond to one of the two devices that will be used in Section V for experimental validation. We choose Harvester A as a universal example in this paper since its structure is very straightforward to describe and model. The structure of Harvester A is shown in Fig. 4(a), and it corresponds directly to the schematic model of Fig. 1. The device can display translation and rotation modes of motion.

B. Self-Consistency Check

As with any model involving multiple physical domains, it is essential to check its self-consistency. In our case, this means that the converted power, the most important figure of merit of a KEH, obtained independently by evaluating the state of the electrical and mechanical domains, must be the same, namely:

$$P_{\text{elec}} = i^2 R_{\text{load}} \quad \text{and} \quad P_{\text{mech}} = \left(\vec{F}_{\text{EM}} \cdot \vec{u} \right). \quad (10)$$

This important aspect of mixed-domain models is explained and tested in Section III-D. In addition, the proposed model will be verified experimentally in Section VI.

C. Simplified Model-Problem With no Mechanical Dynamics to Test Electromagnetic Coupling

Since the full coupled electromechanical model outlined earlier is quite complex, in this Section we propose a simple 'toy' model to check the correctness of our electromagnetic calculations. As a matter of fact, one does not have to consider the dynamical equation (1) in order to understand the electromechanical coupling in this system and quantify Φ and F_{EM}. It would be enough to consider only one loop (instead of a multi-turn coil) and move this loop with a constant velocity relative to a permanent magnet that exerts a magnetic field. For simulations, the parameters of the system are as in Table I and the algorithm of Fig. 3 is applied. We find the e.m.f. and the electromagnetic force acting on the coil as a function of the displacement of the coil with respect to the magnet. We use the power dissipated by the force acting on the loop (P_{elec}) and by force acting on the magnet (P_{mech}) as a figure of merit for self-consistency.

III. ACCURATE CALCULATION OF THE MAGNET FLUX DENSITY

At the core of the original algorithm summarised in Fig. 3 is the calculation of the magnetic flux density $\vec{B}$ in three-dimensions exerted by a permanent magnet. Knowing the vector field $\vec{B}$ allows one to calculate the magnetic flux Φ through a given surface and the force F_{EM}. Three methods to calculate $\vec{B}$ have been implemented and tested.

A. Magnetic Scalar Potential

The magnetic scalar potential (MSP) method is common in simulators that rely on finite-element-methods (FEMs). In the MSP, one solves Poisson's equation in terms of the magnetic field. The main advantage of the MSP combined with FEM is that it is universal and can be applied over a wide range of
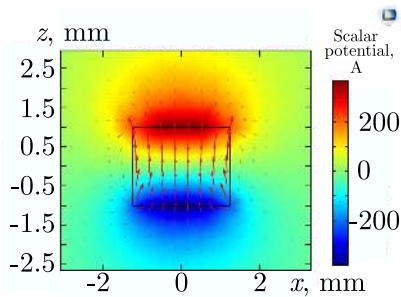
This article has been accepted for inclusion in a future issue of this journal. Content is final as presented, with the exception of pagination.

SOKOLOV *et al.*: MODELLING AND VERIFICATION OF NONLINEAR ELECTROMECHANICAL COUPLING

5

Fig. 5. Magnetic scalar potential and magnetic induction distribution in xz-plane generated by permanent magnet, and modelled in COMSOl multiphysics software.

TABLE II

RESOURCE INTENSITY OF THE COMSOL MODELLING
(EVALUATION ON INTEL CORE I5 7300, 16Gb RAM)

Mesh	Time per configuration, s	Total time, s
Fine	6.5	575
Extra fine	20.7	1865
Extremely fine	109.1	9825

configurations of permanent magnets and magnetic materials. For this reason, it is very common in multi-physics simulators.

This method is implemented in the COMSOL Multiphysics software package [29], and the magnetic field of the corresponding permanent magnet has been modelled with different configurations of a 3D FEM mesh, as shown in Fig. 5. Table II summarises the performance of the FEM method of COMSOL and shows how many resources are required at every step of the calculations. All calculations have been made for a box with zero scalar potential edges and a size of $50 \times 50 \times 50$ mm. We note that a usual modelling step includes approximately a hundred configurations of the relative position of the magnet with respect to the coil. The total amount of data stored in COMSOL for the extremely fine mesh is around 100 Gb, and only this kind of meshing allows one to obtain results of acceptable self-consistency. Hence, the main trade-off of the method is its complexity. This leads to significant resource usage, although we note again that it allows one to solve arbitrary geometry configurations.

B. Array of Magnetic Dipoles

A magnetic dipole (MD) exerts a magnetic field described by the very-well known formula [30], [31]:

$$\vec{B}(\vec{r}) = \frac{\mu_0}{4\pi} \left(\frac{3\vec{r}(\vec{m}_0 \cdot \vec{r})}{r^5} - \frac{\vec{m}_0}{r^3} \right). \quad (11)$$

Here $\vec{r}$ is the radius-vector directed from the MD to the point of observation, μ_0 is the permeability of free space and $\vec{m}_0$ is the magnetic moment of the magnetic dipole. As shown in Fig. 6(a), a permanent magnet can be presented as a collection of small magnetic dipoles [32]. Hence, the magnetic field due to a magnet can be calculated in three-dimensions by applying superposition to magnetic fields generated by individual MDs. The major disadvantage of the method is
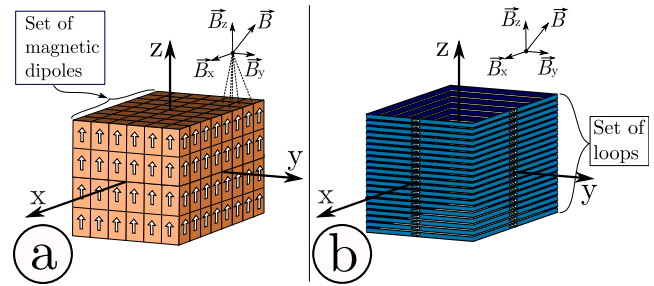

Fig. 6. Representation of a permanent magnet for (a) the magnetic dipole method and (b) the equivalent current method.

that it requires volume integration, which leads to cubic complexity.

However, as was noted in [33], it is possible to reduce dramatically the number of calculations by representing a permanent magnet as a single magnetic dipole. This results in more efficient simulations, in particular for magnets whose geometry possesses symmetry. In the case of a permanent magnet of a relatively complex geometry and a coil which is placed at different locations in space, the magnetic field, and therefore all the following magnetic characteristics of the system, may not be predicted by such an approach in an accurate fashion.

C. Equivalent Coils or Segments With Current

The third approach used in this study to calculate the magnetic flux density $\vec{B}$ employs the well-known expression for the magnetic field due to a line segment [34]:

$$B_s = \frac{\mu_0 i_m}{4\pi d} (\cos \alpha_1 - \cos \alpha_2). \quad (12)$$

Here d is the shortest distance from the point of observation to the line segment and α_1 and α_2 are the respective angles formed by the line and the point of observation. Similar to the previous method, we represent a permanent magnet by a stack of line segments [32], each carrying equivalent current (EC). This replacement is particularly suitable for magnets of symmetrical shapes (cubic or cylindrical), which is the most common case in emKEHs. An example of such a representation is shown in Fig. 6(b) where a cubic magnet is replaced by a set of line segments (or a set of rectangular loops) carrying an equivalent current i_m. The net magnetic field due to such an arrangement can be calculated using the formula above.

The shape and allocation of EC line segments is dictated in a straightforward way by the geometry of a permanent magnet under study. The equivalent current i_m, introduced to mimic the magnetic field of a magnet, must be found from some additional considerations. For instance, tables of data for the magnetisation of different magnetic materials are known. On the other hand, we can always calculate the magnetic field due to a stack of coils with a current i_m. Hence, the current i_m is found so that the magnetic flux density inside the coil stack matches the table data for the flux density of a realistic magnet.
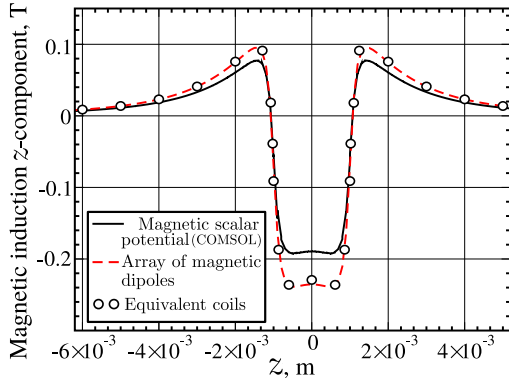
Fig. 7. The z-components of the magnet flux density $\vec{B}(x, y, z)$ for the system described in Table I for $x = 1.4$ mm and $y = 0.7$ mm, evaluated using three different methods.

D. Comparison of the Three Methods and Evaluation of Model Self-Consistency

The performance of all the three methods—magnetic scalar potential, magnetic dipoles and equivalent current—is summarised in Fig. 7, where the z-component of the magnetic flux density $\vec{B}$ is shown. It is easy to see that the magnetic flux density calculated using each of the three methods has the same general dependence on z. However, there are some numerical discrepancies (around 10%) between the results obtained from the MSP method (implemented in COMSOL) and the results obtained from the MD and EC methods. The latter two are completely consistent with each other. The difference in the results for the magnetic flux density $\vec{B}$ calculated using the MSP method and the MD/EC methods is small, but it yields a more significant difference when the magnetic flux and electromagnetic force are obtained from $\vec{B}$.

The model's self-consistency test is performed by calculating the power dissipated in the electrical and mechanical domains. If the simulations are correct, both quantities must be the same according to the power balance principle. We use the 'toy' model described in the previous Section where one coil moves along the z-axis with a constant velocity in the vicinity of a permanent magnet. The relative error of simulations is introduced as follows:

$$\varepsilon = \frac{2 \left| P_{\text{elec}} - P_{\text{mech}} \right|}{\left| P_{\text{elec}} + P_{\text{mech}} \right|} \times 100\%, \tag{13}$$

which is the relative difference in the power dissipated in the electrical and mechanical domains. The formula implies that the error must tend to zero in the ideal case. Figure 8 shows the electrical and mechanical power P_{elec} and P_{mech} and the relative error ε calculated using all the three methods of magnetic field evaluation. The two methods (MD and EC) described in Sections III-B and III-C appear to be self-consistent with a very small difference between P_{elec} and P_{mech}. The MSP method based on FEM simulations is not self-consistent, displaying a large discrepancy between the power in the two domains, while also being most time consuming (42 minutes on an Intel Core i5-7300U CPU, 16 Gb RAM).
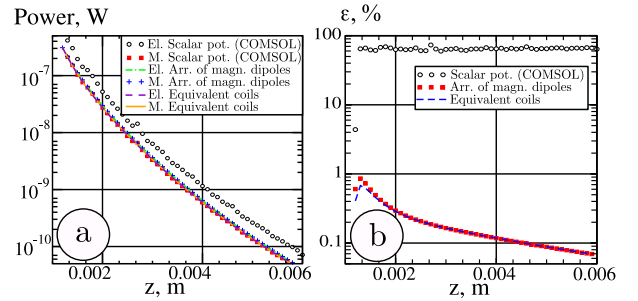

Fig. 8. (a) Power in the mechanical (M.) and electrical (El.) domains as a function of the distance z between the magnet and the coil which defines the strength of coupling, calculated using the three methods of magnetic field evaluation. (b) Relative error ε of the calculation of the converted power using the three methods.
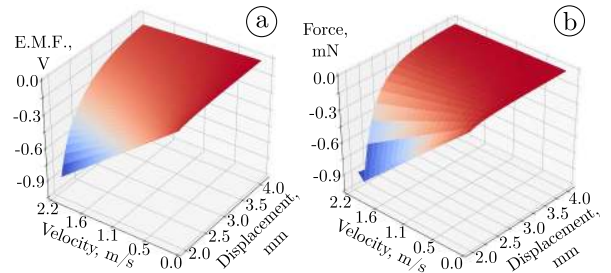
Fig. 9. (a) Electromotive force versus the distance between the magnet and coil and their relative velocity for translational mode. (b) Electromagnetic force versus the distance between the magnet and coil and their relative velocity for translational mode.

IV. ANALYSIS OF ELECTROMAGNETIC COUPLING

With three methods for calculating the vector field $\vec{B}(x, y, z)$ at hand, we can use the algorithm described in Section II-A to complete the lumped model of an emKEH. We note again that as an example of such a harvester we use the device whose parameters are listed in Table I and whose measured data will be used for experimental validation (Harvester A).

Code implementing the algorithm in Fig. 3 has been developed to obtain the simulated data sets. In the case of the translational mode, one is interested in calculating the electromotive force $\mathcal{E}(z, u_z, i)$ and electromagnetic force $F_{\text{EM}}(z, u_z, i)$ as functions of the distance z between the magnet and the coil and the velocity u_z of the magnet with respect to the coil. In the case of the rotational mode, the electromotive force $\mathcal{E}_{\text{rot}}(\varphi, \omega, i)$ and magnetic torque $M_{\text{EM}}(\varphi, \omega, i)$ are calculated as functions of the rotation angle φ and angular velocity ω. These functions are shown in Fig. 9 and Fig. 10 respectively.

In the case of the translational mode (see Fig. 1(b)), we note that these functions are linear with respect to the velocity of the magnet relative to the coil, but nonlinear with respect to the distance between them. The polynomial shape functions are easily obtained through interpolation:

$$\mathcal{E}(z, u_z) = u_z \cdot \left(\sum_{i=0}^{8} a_{\mathcal{E}i} \cdot z^i \right), \tag{14}$$

$$F_{\text{EM}}(z, u_z) = u_z \cdot \left(\sum_{i=0}^{8} a_{Fi} \cdot z^i \right). \tag{15}$$
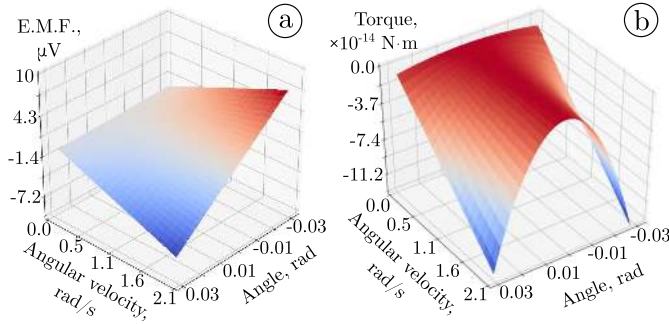
Fig. 10. (a) Electromotive force versus the rotation angle and angular velocity in rotational mode. (b) Magnetic torque versus the rotation angle and angular velocity in rotational mode.

TABLE III

INTERPOLATION COEFFICIENTS FOR TRANSLATIONAL MODE

E.M.F.			Electromagnetic force		
$a_{\mathcal{E}0}$	-1.19×10^3	Vs/m	a_{F0}	-28.5	kg/s
$a_{\mathcal{E}1}$	3.00×10^6	Vs/m^2	a_{F1}	7.31×10^4	kg/(s m)
$a_{\mathcal{E}2}$	-3.30×10^9	Vs/m^3	a_{F2}	-8.19×10^7	kg/(s m^2)
$a_{\mathcal{E}3}$	2.07×10^{12}	Vs/m^4	a_{F3}	5.23×10^{10}	kg/(s m^3)
$a_{\mathcal{E}4}$	8.11×10^{14}	Vs/m^5	a_{F4}	-2.08×10^{13}	kg/(s m^4)
$a_{\mathcal{E}5}$	2.02×10^{17}	Vs/m^6	a_{F5}	5.30×10^{15}	kg/(s m^5)
$a_{\mathcal{E}6}$	-3.14×10^{19}	Vs/m^7	a_{F6}	-8.38×10^{17}	kg/(s m^6)
$a_{\mathcal{E}7}$	2.78×10^{21}	Vs/m^8	a_{F7}	7.54×10^{19}	kg/(s m^7)
$a_{\mathcal{E}8}$	-1.07×10^{23}	Vs/m^9	a_{F8}	-2.96×10^{21}	kg/(s m^8)

The interpolation coefficients $a_{\mathcal{E}i}$ and a_{Fi} are given in Table III. The shape functions do not change if one alters the parameters of the systems from Table I. However, changing the shape of the magnet or the coil may change the shape functions, but they can be easily recalculated using the developed algorithm.

The same algorithm is applied to the case of the rotational mode of the resonator (see Fig. 1(c)). To simplify the calculations, we solve a problem that is mechanically equivalent to the original problem, but in this case the coil rotates with respect to the magnet. Figure 10(a) and Fig. 10(b) show that the e.m.f and magnetic torque are also linear with respect to the angular velocity (the counterpart of velocity in the translational mode) and nonlinear with respect to the rotation angle (the counterpart of displacement in translational mode). These functions are also found using interpolation:

$$\mathcal{E}_{\text{rot}}(\varphi, \omega) = \omega \cdot \left(\sum_{i=0}^{4} b_{\mathcal{E}2i+1} \cdot \varphi^{2i+1} \right), \quad (16)$$

$$M_{\text{EM}}(\varphi, \omega) = \omega \cdot \left(\sum_{i=0}^{3} b_{F2i} \cdot \varphi^{2i} \right). \quad (17)$$

The interpolation coefficients $b_{\mathcal{E}2i+1}$ and b_{F2i} are given in Table IV.

We want to highlight that the electromotive force represents electromechanical coupling in emKEHs in the electrical domain while the electromagnetic force does so in the mechanical domain. The analysis of the obtained e.m.f. and electromagnetic force shows that, as expected, strong coupling between the domains exists in the translational mode and it is

TABLE IV

INTERPOLATION COEFFICIENTS FOR ROTATION MODE

E.M.F.			Electromagnetic torque		
$b_{\mathcal{E}1}$	-4.99×10^{-4}	Vs	b_{M0}	-3.20×10^{-16}	kg m^2/s
$b_{\mathcal{E}3}$	-3.93×10^{-3}	Vs	b_{M2}	-1.30×10^{-9}	kg m^2/s
$b_{\mathcal{E}5}$	1.69×10^{-2}	Vs	b_{M4}	-2.06×10^{-8}	kg m^2/s
$b_{\mathcal{E}7}$	-2.96×10^{-2}	Vs	b_{M6}	1.51×10^{-8}	kg m^2/s
			b_{M8}	3.08×10^{-7}	kg m^2/s
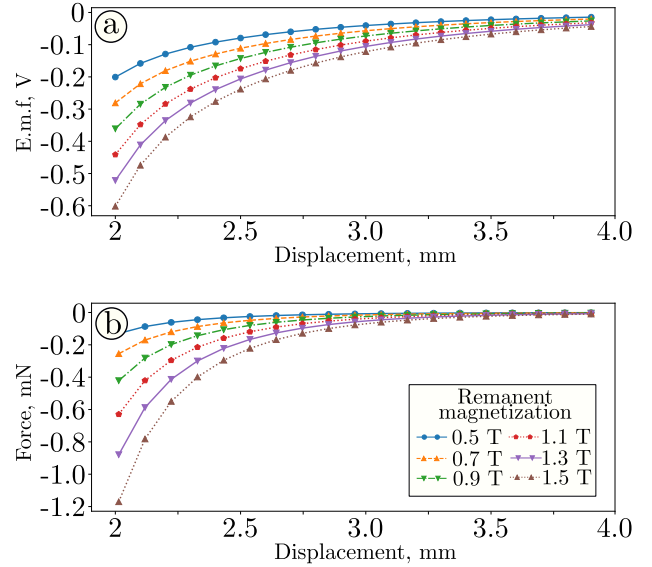
Fig. 11. Cross-sections of the surfaces presented in Fig. 9. (a) Shape functions $\mathcal{E}(z, u_z)$ taken at fixed $v_z = 1.0$ m/s. (b) Shape functions $F_{\text{EM}}(z, u_z)$ taken at fixed $v_z = 1.0$ m/s. In this graph we show how the shape functions change depending on different magnetisations of the magnet.

very weak in the rotational mode. This can be understood by noting that both quantities depend on the slope of the magnetic flux (see expressions (5) and (6)), and the slope of the magnetic flux with respect to the rotation angle drops significantly (as shown in Fig. 10) when a rotational mode of motion is actuated by external driving.

We also observe another extremely useful property of the system. The shape functions can be easily scaled to fit any given magnetic material used as the harvester's magnetic proof-mass. The magnetic properties of the proof-mass are defined by the residual magnetization B_{res}. In the proposed method, it is proportional to the current density i_{m} in the equivalent coil. Therefore, the magnetic flux density B, the magnetic flux Φ and, finally, the e.m.f. $\mathcal{E}$ are all proportional to the magnetisation B_{res}:

$$\frac{\mathcal{E}_2}{\mathcal{E}_1} = \frac{B_{\text{res}\,2}}{B_{\text{res}\,1}}. \quad (18)$$

The linear scaling of the shape functions is clearly seen in Fig. 11(a) and Fig. 12(a).

The electromagnetic force and the magnetic torque, on the other hand, depend both on the e.m.f. and the magnetic flux density. Thus, they are scaled quadratically with respect to the

This article has been accepted for inclusion in a future issue of this journal. Content is final as presented, with the exception of pagination.

8

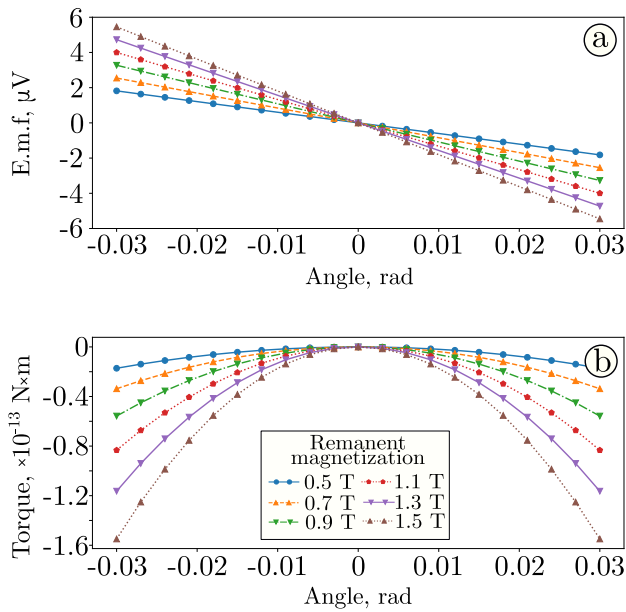IEEE TRANSACTIONS ON CIRCUITS AND SYSTEMS–I: REGULAR PAPERS

Fig. 12. Cross-sections of the surfaces presented in Fig. 9. (a) Shape functions $\mathcal{E}_{\text{rot}}(\varphi, \omega)$ taken at fixed $\omega = 1.0$ rad/s. (b) Shape functions $M_{\text{EM}}(\varphi, \omega)$ taken at fixed $\omega = 1.0$ rad/s. In this graph we show how the shape functions change depending on different magnetisations of the magnet.

residual magnetisation of the magnet:

$$\frac{B_{\text{res 2}}}{B_{\text{res 1}}} = \left(\frac{F_{\text{EM 2}}}{F_{\text{EM 1}}}\right)^2 = \left(\frac{M_2}{M_1}\right)^2. \tag{19}$$

The quadratic scaling can be seen in Fig. 11(b) and Fig. 12(b). Therefore, when solving an optimisation problem to find the optimal magnetisation of the proof-mass to enhance electro-mechanical coupling in electromagnetic harvesters, it is not required to use the algorithm of Fig. 3 for different magnetic materials. It should be used only once, and then the results should be multiplied by an appropriate scaling factor. This dramatically reduces the computational time needed to optimize the system.

With the shape functions and the scaling factors identified, we have a self-consistent lumped model of a harvester. The proposed lumped model is verified experimentally in the next Section.

V. DESCRIPTION OF THE EXPERIMENTAL SET-UP AND EXPERIMENT METHODOLOGY

The experimental verification of the proposed modelling methodology has been carried out using two MEMS electromagnetic harvesters, denoted Harvester A and Harvester B, whose structures and allocations of the permanent magnets with respect to the coils are very different. The experimental set-up is shown in Fig. 13, and the arrangement of the experiment is the same for both devices. The schematic structures of the two harvesters are shown in Fig. 4. In this Section we make a direct comparison between the experiment and the model. We also note that the modelling approach is not limited to this configuration and can be applied to many micro- and macroscopic electromagnetic harvesters [11], [27], [35].
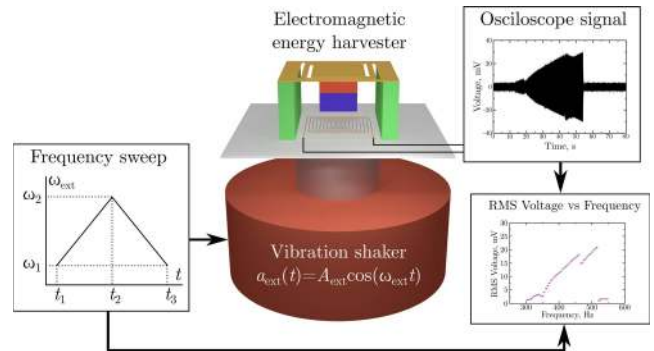

Fig. 13. Methodology of the experiment and the experimental set-up for the voltage-frequency characterisation.
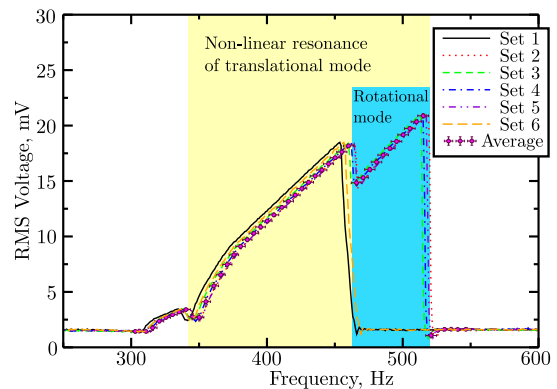

Fig. 14. Processed experimental data of the forward sweep branch of the electromagnetic energy harvester showing the voltage induced in the device as a function of the actuation frequency at $A_{\text{ext}} = 3.0$ m/s^2.

The experiment consists of a shaking platform which vibrates with a controlled sinusoidal acceleration whose magnitude A_{ext} and frequency f_{ext} can be set up as desired. It is very typical for such an experiment to use an acceleration pattern with fixed A_{ext} but with $f_{\text{ext}}(t)$ changing linearly in time. This change is slow enough so we can assume that the system in quasi steady-state. Usually, the acceleration pattern is such that f_{ext} increases and then it decreases, as shown in the Fig. 12. This mimics the so-called forward and backward sweeps of the actuation frequency, allowing us to detect hysteresis in nonlinear systems, which is particularly relevant for Harvester A. The induced voltage generated in the energy harvester under test is recorded by an oscilloscope with a resolution of $\Delta t = 2 \times 10^{-4}$ s. Thus, a number of data sets of the induced voltage (the e.m.f. taken with the minus sign) versus time $V_i = V(t_i)$ are obtained at different settings of A_{ext} with and without an electrical load (load resistor). It should be noted that the mechanical state (displacement or rotation angle) cannot be observed directly, and we can monitor only the electrical state of the system.

Since Harvester A is a nonlinear device prone to switching between different modes of motion, multiple experiments have been run and recorded in order to have statistical repeatability and to estimate the uncertainty of the experiment for the same acceleration amplitude. For further comparison with the theory and modelling, we have kept six data sets for each A_{ext}. A typical example of the six measured data sets for given A_{ext} is shown in Fig. 14 (where the matching

This article has been accepted for inclusion in a future issue of this journal. Content is final as presented, with the exception of pagination.

SOKOLOV *et al.*: MODELLING AND VERIFICATION OF NONLINEAR ELECTROMECHANICAL COUPLING

9

of the actuation frequency and time has been already done, as described below). As can be seen from the figure, the data sets are not always the same, even though the parameters of the experiment are the same. The high-voltage branch occurs in the region of bi-stability, and the device, when driven to that branch, is sensitive to small perturbations. From the high-voltage branch (corresponding to the translational mode) it can drop to a lower branch (corresponding to mixed translational and rotational modes, also bi-stable) or to the lowest branch (translational mode again). We note that since the actuation frequency A_{ext} is swept over a wide range of values, it is possible to observe resonances associated with multiple spatial eigen-modes, as explained in Section II. However, since the system is nonlinear, its bandwidth becomes wide as a result. The resonances of eigen-modes are not clearly distinctive, and often the resonance response of one eigen-mode (for instance, translational mode) overlaps with the resonance response of another mode (for example, rotational mode). This is what is seen in Fig. 14.

It should be noted that the obtained data sets, although measured at the same parameters, may be shifted by some Δf_{ij} due to different initial conditions, and for this reason cannot be simply averaged. We also want to avoid the situation where two different data sets (as, for example, set 1 and set 6 from Fig. 14) are used for the comparison with the model. Hence, in order to perform a correct comparison between the measured data and modelled results, we use the following approach to pre-process the experimental data:

☐ Match time t with the frequency $f_{\text{ext}}(t)$ for each of the data sets using their Fast Fourier Transform (FFT) spectra.

☐ Calculate the RMS voltage for each data set for a given time window T_w:

$$V_{\text{RMS}} = \sqrt{1/T_w \int_{t_i}^{t_i+T_w} V_i^2 \mathrm{d}t}$$

and exclude the unsuitable set(s).

☐ Match all the sets by their frequency shifts Δf_{ij} using the least squares method, i.e., by minimising the cost function:

$$\sum_k \left[V_i(f_k) - V_j(f_k + \Delta f_{ij}) \right]^2.$$

☐ Calculate the average RMS voltage $\langle V_{\text{RMS}} \rangle$ and the measurement errors Δf and ΔV_{RMS}. The error Δx of a signal x is calculated using the formula $\Delta x = 3.1 \cdot \sigma_x / \sqrt{N}$ where σ_x is the standard deviation of this signal waveform, N is the number of samples in it and 3.1 is the Student's distribution coefficient providing the authenticity 95%.

The measured and processed data are used to compare the experiment with the model.

VI. EXPERIMENTAL VERIFICATION

A. Verification Using Harvester A

The comparison of the theory and modelling with the experiment begins by verifying the parameters of the harvester.

TABLE V
MECHANICAL PARAMETERS OF HARVESTER A
RECONSTRUCTED FROM THE EXPERIMENT

Parameter	Value	
Air damping coefficient c_a	3.39×10^{-3}	kg/s
Quality factor $Q = \sqrt{mk}/c_a$	69.2	
Linear spring coefficient k	556.59	N/m
Cubic spring coefficient k_3	-8.1×10^{10}	N/m³
Fifth-order spring coefficient k_5	1.19×10^{21}	N/m⁵
Seventh-order spring coefficient k_7	-2.90×10^{29}	N/m⁷
Moment of inertia of the resonator I	5.17×10^{-10}	kg m
Torsional stiffness k'	4.02×10^{-3}	N m
Torsional air damping coefficients c_a'	3.45×10^{-4}	N m s

While some of these are known (for instance, the mass of the resonator or its natural frequency, see Table I), others are not known and cannot be predicted from the design and simulation stage (for instance, the nonlinear spring coefficients). The mechanical parameters, including the nonlinear spring coefficients (k, k_3, k_5 and k_7) and the quality factor Q, are calculated from the experimental data obtained when the electrical load is disconnected. The optimization procedure uses the standard least square differences technique with the cost function:

$$\min \sum_{i=1}^{N} \left(V_{\text{RMS}}^{\text{theor}} - V_{\text{RMS}}^{\text{exp}} \right)^2. \tag{20}$$

The mechanical parameters that were not known but reconstructed from the experiment are summarised in Table V.

The proposed model, based on the theory summarised in equations (1) to (9) with the shape functions (14) to (17), is solved numerically using a standard scheme (a Runge-Kutta method) and analytically using the Harmonic Balance Method (HBM). The results are compared with the experiment and presented in Fig. 15. This graph shows the experimental data, processed as described in Section V, in the form of the induced RMS voltage as a function of external driving frequency f_{ext}. The graphs have a typical shape of nonlinear resonance due to the mechanical nonlinearity of the spring supporting the oscillating magnetic proof-mass. Two frequency sweeps, forward and backward, are shown in the figure to demonstrate the bi-stability of the system. The mechanical nonlinearity leads to a wideband frequency response of the harvesters, as desired for these type of devices. As an additional reference, the graph shows the amplitude A_0 of the linear response $A_0(f_{\text{ext}})$ that would be expected in the system if it were linear:

$$A_0 = \frac{m A_{\text{ext}}}{(k^2 - m\omega_{\text{ext}}^2)^2 + \omega_{\text{ext}}^2 c_a^2}. \tag{21}$$

In the above formula, $\omega_{\text{ext}} = 2\pi f_{\text{ext}}$. The linear response allows us to cross-validate the air damping coefficient c_a and the quality factor Q of the system. The result of the model and the experimental results are in a very good agreement, validating the theory presented in this paper.

The additional use of the HBM to solve the model equations is a significant advantage compared to the sole use of a numerical integration technique. The HBM is not resource intensive, and, in addition, it provides another tool for verification as we deal with a nonlinear system. The fact that the HBM and
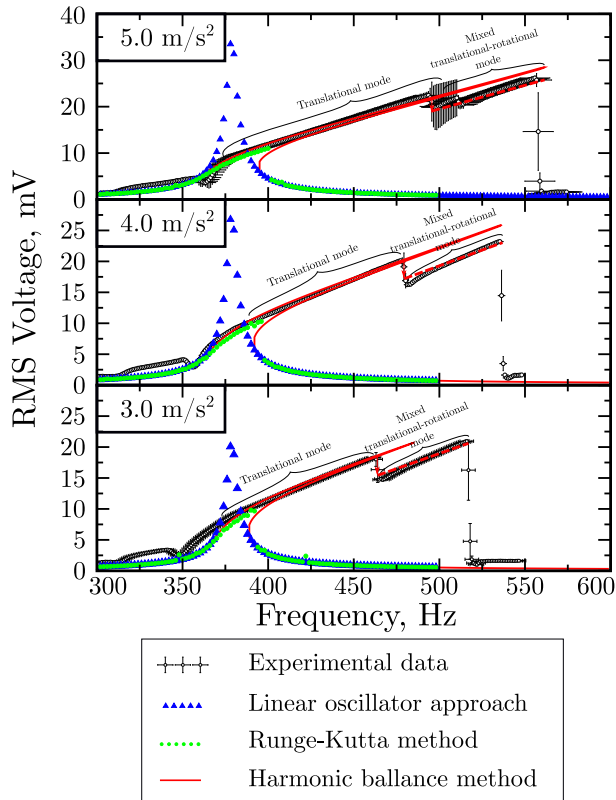
Fig. 15. Experimentally measured RMS voltage V_{RMS} (black circles with error bars) as a function of the actuation frequency A_{ext} compared to the proposed model (green circles). For reference, a semi-analytical Harmonic Balance Method is also shown (red lines) together with the linear response (21) (blue triangles). The data is measured at three different external acceleration amplitudes: 3 m/s^2, 4 m/s^2 and 5 m/s^2 respectively.
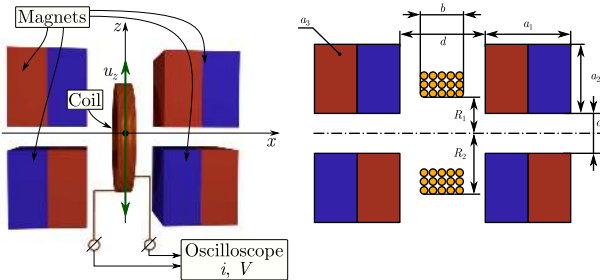

Fig. 16. The schematic drawing of the kinetic energy harvester Model B. It consist of the array of the four identical permanent magnets and the cylindrical multi-layer coil.

the Runge-Kutta methods are consistent with each other and with the experimental data speaks towards the validity of the model and the techniques to solve the model. We also point out that the experimental results contain the responses associated with both translational and rotational modes, as highlighted in Fig. 15. All such modes can be accommodated in the presented theory.

B. Verification Using Harvester B

The second device used to demonstrate the applicability of our approach is shown in Fig. 4(b), with the details outlining its geometry presented in Fig. 16. This system consists of

TABLE VI
KNOWN PHYSICAL PARAMETERS OF HARVESTER B

Parameter	Value	
Mass of the resonator m	2.9×10^{-3}	kg
Length of the permanent magnets a_1	8.0×10^{-3}	m
Height of the permanent magnets a_2	2.0×10^{-3}	m
Width of the permanent magnets a_3	4.0×10^{-3}	m
Vertical distance between magnets c	2.4×10^{-4}	m
Horizontal distance between magnets d	2.0×10^{-3}	m
Thickness of the coil b	1.0×10^{-3}	m
Internal radius of the coil R_1	5.75×10^{-4}	m
External radius of the coil R_2	3.25×10^{-3}	m
The number of turns N	2500	
Resistance of the coil and oscilloscope R	3.114×10^3	Ω

TABLE VII
MECHANICAL PARAMETERS OF HARVESTER B RECONSTRUCTED FROM THE EXPERIMENT

Parameter	Value	
Air damping coefficient c	0.026	kg/s
Linear restoring force coefficient k	404.1	N/m
Third order restoring force coefficient k_3	1.76×10^6	N/m^3

an array of permanent magnets and a movable cylindrical coil which oscillates in the magnetic field generated by the fixed magnets. It is interesting to note that this arrangement idea is opposite to Harvester A where, by contrast, a square magnet is attached to elastic nonlinear springs and oscillates in the vicinity of a fixed multi-layered square coil under external driving. The known physical parameters of Harvester B are listed in Table VI. As in the case of Harvester A, some mechanical parameters are unknown, including the air damping and nonlinear spring coefficients; these have to be extracted from the experimental data in the same fashion as described in the previous Section. These parameters are calculated from experimental characteristics using an optimization procedure with a standard least square differences technique when the electrical load is disconnected. We reiterate that these parameters cannot be predicted at the design stage (in particular for nonlinear MEMS) or measured directly. Hence, some indirect procedure of extraction must be employed. The additional parameters reconstructed from the experiment are give in Table VII.

The algorithm proposed in Section II can also be applied to model a system of the configuration described above. We note that the complexity of modelling in this case increases since we have to model four permanent magnets and a coil that has 2500 turns. Nevertheless, such modelling is feasible, and the lumped expressions for the e.m.f and the z-component of the electromagnetic force can be obtained:

$$\mathcal{E}(v, z) = v\left(e_0 + e_2 z^2 + e_4 z^4 + e_6 z^6 + e_8 z^8 + e_{10} z^{10}\right).$$
(22)

$$F_{\text{em}}(v, z) = v\left(f_0 + f_2 z^2 + f_4 z^4 + f_6 z^6 + f_8 z^8 + f_{10} z^{10}\right).$$
(23)

Here, e_i and f_i are the interpolation parameters, and their numerical values for Harvester B are summarised

This article has been accepted for inclusion in a future issue of this journal. Content is final as presented, with the exception of pagination.

SOKOLOV *et al.*: MODELLING AND VERIFICATION OF NONLINEAR ELECTROMECHANICAL COUPLING
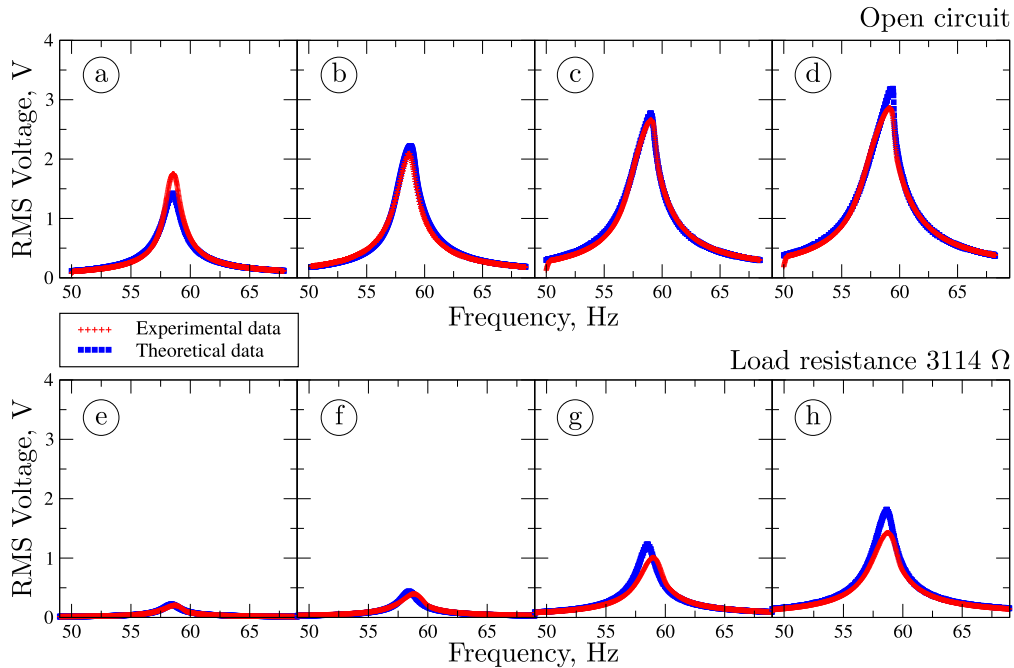
11

Fig. 17. Resonance curves of Harvester B (experimental data shown by red and modelled data shown by blue) in the form of RMS voltage as a function of the frequency f_{ext} of external driving. The top row shows the results for the open-circuit measurement (without electromechanical coupling) at accelerations of $0.3\,g$, $0.5\,g$, $0.8\,g$ and $1.0\,g$. The bottom row shows the results for the system with an electrical load of $R_L = 3114\,\Omega$ (with electromechanical coupling) at the same acceleration levels.

TABLE VIII

INTERPOLATION COEFFICIENTS FOR THE TRANSLATIONAL
MODE OF HARVESTER B

E.M.F.			Electromagnetic torque		
e_0	6.17	Vs/m	f_0	-0.0122	kg/s
e_2	-2.24×10^6	Vs/m^3	f_2	8.88×10^3	kg/(s m^2)
e_4	1.38×10^{11}	Vs/m^5	f_4	-2.20×10^9	kg/(s m^4)
e_6	1.69×10^{16}	Vs/m^7	f_6	1.82×10^{14}	kg/(s m^6)
e_8	-4.06×10^{21}	Vs/m^9	f_8	7.47×10^{18}	kg/(s m^8)
e_{10}	2.65×10^{26}	Vs/m^{11}	f_{10}	-1.65×10^{24}	kg/(s m^{10})

in Table VIII. For the obtained lumped expressions, we have performed the self-consistency test as described in the earlier Section and have calculated the magnetisation of the magnetic material as a function of the relative speed of the coil and the magnets, similar to Fig. 9 and Fig. 11 presented in Section IV.

Finally, knowing the parameters of the electromagnetic coupling in Harvester B, we can make a direct comparison between its modelling and experimental characterisation, as shown in Fig. 17. This figure presents a comparison between the measured (red points) and modelled (blue points) RMS voltage as a function of the frequency f_{ext} of external vibrations with and without an electrical load. The four figures in each row correspond to four amplitudes A_{ext} of external vibrations ($0.3\,g$, $0.5\,g$, $0.8\,g$ and $1.0\,g$). The top row shows the results without an electrical load (without electromechanical coupling) while the bottom row shows the results with an electrical load of $R_L = 3114\,\Omega$ (with electromechanical coupling) at the same accelerations levels. Firstly, we note that, as expected, increasing A_{ext} results in larger RMS voltage generated in the system. Secondly, it can be clearly seen

that adding an electrical load results in electromechanical coupling and energy transfer from the mechanical to the electrical domain. The presence of the electromagnetic force is seen as an additional dissipation (damping) force reducing the amplitude of the resonance characteristic. We note that the measured and modelled data show very good agreement, and the minor discrepancy may be caused by some natural uncertainties of measurements.

VII. CONCLUSIONS

This paper proposed an accurate theory allowing one to model electromagnetic coupling in kinetic energy harvesters. The usual approach used in the literature reduces the electromagnetic coupling to a linear damper when one models such devices. However, due to the nature of the magnetic flux density and magnetic flux, the coupling is nonlinear, and its incorrect use may result in significant errors. We showed how first principles of electromagnetics can be applied to a electromagnetic kinetic energy harvester and how they result in a reduced order lumped model through the use of shape functions. The obtained lumped model is fully compatible with the ordinary differential equation describing the mechanical dynamics of the magnetic proof-mass and the Kirchhoff Voltage Law describing the electrical state of the system. The presented methodology was verified experimentally for two qualitatively different emKEH topologies. We described the design of the experiment and the data processing method in detail, since, as usual with MEMS devices, we could readily have access only to the electrical parameters of the system. Following this approach, experimental data was acquired, processed and compared with the developed model. Since we

This article has been accepted for inclusion in a future issue of this journal. Content is final as presented, with the exception of pagination.

12   IEEE TRANSACTIONS ON CIRCUITS AND SYSTEMS–I: REGULAR PAPERS

dealt with a nonlinear system, a range of tools to solve nonlinear differential equations were used to ensure that the solution we obtained was indeed correct. The comparison between the model and the experiment shows very good agreement, and we conclude that the methodology proposed in this paper is accurate and verified.

REFERENCES

[1] S. P. Beeby and T. O'Donnell, *Energy Harvesting Technologies*. Boston, MA, USA: Springer, 2009.

[2] O. Brand, G. K. Fedder, C. Hierold, J. G. Korvink, and O. Tabata, *Micro Energy Harvesting*. Hoboken, NJ, USA: Wiley, 2015.

[3] E. Blokhina, A. El Aroudi, E. Alarcon, and D. Galayko, *Nonlinearity in Energy Harvesting Systems Micro- and Nanoscale Applications*. Berlin, Germany: Springer, 2016.

[4] B. Yang *et al.*, "Electromagnetic energy harvesting from vibrations of multiple frequencies," *J. Micromech. Microeng.*, vol. 19, no. 3, 2009, Art. no. 035001.

[5] S. P. Beeby, R. N. Torah, M. Tudor, P. Glynne-Jones, T. O'Donnell, C. R. Saha, and S. Roy, "A micro electromagnetic generator for vibration energy harvesting," *J. Micromech. Microeng.*, vol. 17, no. 7, p. 1257, Jun. 2007.

[6] M. A. Halim, R. Rantz, Q. Zhang, L. Gu, K. Yang, and S. Roundy, "An electromagnetic rotational energy harvester using sprung eccentric rotor, driven by pseudo-walking motion," *Appl. Energy*, vol. 217, pp. 66–74, May 2018.

[7] S. Sun, X. Dai, K. Wang, X. Xiang, G. Ding, and X. Zhao, "Nonlinear electromagnetic vibration energy harvester with high efficient closed magnetic circuit," *IEEE Magn. Lett.*, vol. 9, 2018, Art. no. 6102604.

[8] D. Mallick, A. Amann, and S. Roy, "High figure of merit nonlinear microelectromagnetic energy harvesters for wideband applications," *J. Microelectromech. Syst.*, vol. 26, no. 1, pp. 273–282, 2017.

[9] K. J. Kim, F. Cottone, S. Goyal, and J. Punch, "Energy scavenging for energy efficiency in networks and applications," *Bell Labs Tech. J.*, vol. 15, no. 2, pp. 7–29, Sep. 2010.

[10] R. L. Harne and K. Wang, "A review of the recent research on vibration energy harvesting via bistable systems," *Smart Mater. Struct.*, vol. 22, Sep. 2013, Art. no. 023001.

[11] Y. Tan, Y. Dong, and X. Wang, "Review of MEMS electromagnetic vibration energy harvester," *J. Microelectromech. Syst.*, vol. 26, no. 1, pp. 1–16, Feb. 2017.

[12] D. Mallick, A. Amann, and S. Roy, "Surfing the high energy output branch of nonlinear energy harvesters," *Phys. Rev. Lett.*, vol. 117, no. 19, Nov. 2016, Art. no. 197701.

[13] H. Liu, Y. Qian, and C. Lee, "A multi-frequency vibration-based MEMS electromagnetic energy harvesting device," *Sens. Actuators A, Phys.*, vol. 204, pp. 37–43, Dec. 2013.

[14] H. Liu, B. W. Soon, N. Wang, C. J. Tay, C. Quan, and C. Lee, "Feasibility study of a 3D vibration-driven electromagnetic MEMS energy harvester with multiple vibration modes," *J. Micromech. Microeng.*, vol. 22, no. 12, Nov. 2012, Art. no. 125020.

[15] F. Cottone, R. Frizzell, S. Goyal, G. Kelly, and J. Punch, "Enhanced vibrational energy harvester based on velocity amplification," *J. Intell. Mater. Syst. Struct.*, vol. 25, no. 4, pp. 443–451, Mar. 2014.

[16] E. Boco, V. Nico, D. O'Donoghue, R. Frizzell, G. Kelly, and J. Punch, "Optimization of coil parameters for a nonlinear two Degree-of-Freedom (2DOF) velocity-amplified electromagnetic vibrational energy harvester," in *Proc. Int. Conf. Smart Cities Green ICT Syst.*, May 2015, pp. 1–10.

[17] J. M. Oliver and S. Priya, "Design, fabrication, and modeling of a four-bar electromagnetic vibration power generator," *J. Intell. Mater. Syst. Struct.*, vol. 21, no. 13, pp. 1303–1316, Sep. 2010.

[18] Q. Zhang and E. S. Kim, "Microfabricated electromagnetic energy harvesters with magnet and coil arrays suspended by silicon springs," *IEEE Sensors J.*, vol. 16, no. 3, pp. 634–641, Feb. 2016.

[19] A. Sokolov, D. Mallick, S. Roy, M. P. Kennedy, and E. Blokhina, "Novel approach to modelling electromechanical coupling and testing its self-consistency in micro-scale kinetic electromagnetic energy harvesters," in *Proc. IEEE Int. Conf. Electron., Circuits Syst. (ICECS)*, Dec. 2018, pp. 405–408.

[20] K. F. Graff, *Wave Motion in Elastic Solids*. Chelmsford, MA, USA; Courier Corporation, 2012.

[21] J. A. Pelesko and D. H. Bernstein, *Modeling MEMS and NEMS*. Boca Raton, FL, USA: CRC Press, 2002.

[22] A. H. Nayfeh, M. I. Younis, and E. M. Abdel-Rahman, "Reduced-order models for MEMS applications," *Nonlinear Dyn.*, vol. 41, no. 1, pp. 211–236, 2005.

[23] Y. C. Liang, W. Z. Lin, H. P. Lee, S. P. Lim, K. H. Lee, and H. Sun, "PROPer orthogonal decomposition and its applications—Part II: Model reduction for MEMS dynamical analysis," *J. Sound Vib.*, vol. 256, no. 3, pp. 515–532, Sep. 2002.

[24] E. M. Abdel-Rahman, M. I. Younis, and A. H. Nayfeh, "Characterization of the mechanical behavior of an electrically actuated microbeam," *J. Micromech. Microeng.*, vol. 12, no. 6, p. 759, 2002.

[25] J. Ricart *et al.*, "Control of MEMS vibration modes with pulsed digital oscillators—Part II: Simulation and experimental results," *IEEE Trans. Circuits Syst. I, Reg. Papers*, vol. 57, no. 8, pp. 1879–1890, Aug. 2010.

[26] W. Zhang, R. Baskaran, and K. L. Turner, "Effect of cubic nonlinearity on auto-parametrically amplified resonant MEMS mass sensor," *Sens. Actuators A, Phys.*, vol. 102, pp. 139–150, Dec. 2002.

[27] D. Mallick, A. Amann, and S. Roy, "A nonlinear stretching based electromagnetic energy harvester on FR4 for wideband operation," *Smart Mater. Struct.*, vol. 24, no. 1, Nov. 2014, Art. no. 015013.

[28] L. D. Landau and E. M. Lifshitz, *Mechanics and Electrodynamics*. Amsterdam, The Netherlands: Elsevier, 2013.

[29] *The Finite Element Method (FEM)*. Accessed: Feb. 21, 2017. [Online]. Available: https://www.comsol.com/multiphysics/finite-element-method

[30] S. D. Sadatian, "Simulation the distribution of electrical charges fields," *Amer. J. Math. Comput. Model.*, vol. 2, no. 3, pp. 76–83, Aug. 2017.

[31] T. L. Chow, *Introduction to Electromagnetic Theory: A Modern Perspective*. Burlington, MA, USA: Jones Bartlett Learning, 2006.

[32] H. A. Haus and J. R. Melcher, *Electromagnetic Fields and Energy*. Upper Saddle River, NJ, USA: Prentice-Hall, 1989.

[33] A. J. Sneller and B. P. Mann, "On the nonlinear electromagnetic coupling between a coil and an oscillating magnet," *J. Phys. D, Appl. Phys.*, vol. 43, no. 29, Jul. 2010, Art. no. 295005.

[34] C. R. Paul and S. A. Nasar, *Introduction to Electromagnetic Fields*. New York, NY, USA: McGraw-Hill, 1987.

[35] E. O'Riordan, R. Frizzell, D. O'Connell, and E. Blokhina, "Characterisation of anti-resonance in two-degree-of-freedom electromagnetic kinetic energy harvester, with modified electromagnetic model," *J. Intell. Mater. Syst. Struct.*, vol. 29, no. 10, pp. 2295–2306, Mar. 2018.

Andrii Sokolov (S'18) received the B.Sc. degree in computational physics and the M.Sc. degree in theoretical physics from Odessa National I.I. Mechnikov University, Ukraine, in 2009 and 2010, respectively. He joined the Ph.D. Program in the School of Electrical and Electronic Engineering, University College Dublin, Ireland, in 2018. His research interests are vibration-based energy harvesters.

Dhiman Mallick (M'12) received the B.Sc. degree (Hons.) in physics and the B.Tech. (Post-Graduate) and M.Tech. degrees in radio physics and electronics engineering from the University of Calcutta, in 2007, 2010, and 2012, respectively, and the Ph.D. degree in electrical and electronic engineering from Tyndall National Institute, University College Cork, in February 2017. Before that, he was a Post-Doctoral Researcher with the Tyndall National Institute, Ireland. He is currently an Assistant Professor with the Department of Electrical Engineering, Indian Institute of Technology Delhi (IITD), New Delhi, India. Till date, he has authored/coauthored 40 published articles in peer-reviewed journals and conference proceedings, one book chapter and one patent (filed). His research interests include MEMS, NEMS, energy harvesting, and wireless power transfer.

This article has been accepted for inclusion in a future issue of this journal. Content is final as presented, with the exception of pagination.

SOKOLOV *et al.*: MODELLING AND VERIFICATION OF NONLINEAR ELECTROMECHANICAL COUPLING 13

Saibal Roy received the M.Sc. degree in physics from the Indian Institute of Technology (IIT) Khraragpur, Khraragpur, India, in 1987, and the Ph.D. degree in physics/materials science from IACS, in 1994.

In 2013, he was invited in a sabbatical position hosted by Electrical Engineering Department and supported by Materials Science Department, Stanford University. He is currently a Research Professor with the Department of Physics, University College Cork (UCC), and the Head of Micropower Systems and Nanomagnetics Research Group, Tyndall National Institute, Ireland. To date, he has three granted global patents, written seven book chapters and published over 180 articles in leading journals and conference proceedings, with over 5000 international citations and h index of 33 to date. Within the last decade, he was able to bring over €eight Million competitive research grants focusing these areas. Some of his published works on 'Miniaturized/MEMS vibrational energy harvesting through EMT' have received over 1000 citations to date and featured widely in international media. On the other hand, Tyndall 'Magnetics on Si' team successfully licensed the micro-transformer/inductor technology recently with a substantial license fee (over €1Million) to two major multinational companies.

Prof. Roy has served as a member of several programme committees, chaired sessions and delivered invited talks in many International Conferences & Corporate R&Ds. In 2015, he was awarded the 'A. S. Paintal visiting Chair Professorship' in Engineering by INSA (Indian National Science Academy). The award was given to three outstanding foreign scientists in that year. He is also holding Science Foundation Ireland (SFI) Principal Investigator (PI) Grant Award and also a Funded Investigator in SFI €39 Million Research Center on 'Internet of Things - CONNECT'. In recognition, the team was awarded as the Research Team by the University (UCC), in 2015. This was in recognition for the contribution, he made in the field of Thin-films, micro-nano-magnetics, Micro/Nano Technologies, and Sciences over previous 20 years.

Michael Peter Kennedy (S'84–M'91–SM'95–F'98) received the B.E. degree in electronics from the National University of Ireland, Dublin, in 1984, and the M.S. and Ph.D. degrees from the University of California (UC Berkeley), Berkeley, in 1987 and 1991, and the D.Eng. degree from the National University of Ireland, in 2010.

He was a Design Engineer with Philips Electronics, a Post-Doctoral Research Engineer with the Electronics Research Laboratory, UC Berkeley, and as a Professeur Invité with the Federal Institute of Technology Lausanne (EPFL), Switzerland. From 1992 to 2000, he was on the Faculty of the Department of Electronic and Electrical Engineering, University College Dublin (UCD), Dublin, Ireland, where he taught electronic circuits and computer-aided circuit analysis and directed the undergraduate Electronics Laboratory. In 2000, he joined University College Cork (UCC), Cork, Ireland, as a Professor and the Head of the Department of Microelectronic Engineering. He was the Dean of the Faculty of Engineering, UCC, from 2003 to 2005, and the Vice-President for Research, from 2005 to 2010. He returned to UCD as a Professor of microelectronic engineering, in 2017, where he is currently the Head of the School of Electrical and Electronic Engineering.

Dr. Kennedy was contributions to the study of Neural Networks and Nonlinear Dynamics. He was a recipient of the 1991 Best Paper Award from the International Journal of Circuit Theory and Applications and the Best Paper Award at the European Conference on Circuit Theory and Design 1999. He served as an Associate Editor for the IEEE TRANSACTIONS ON CIRCUITS AND SYSTEMS, from 1993 to 1995 and from 1999 to 2004. He was awarded the IEEE Third Millennium Medal, the IEEE Circuits and Systems Society Golden Jubilee Medal, in 2000, and the inaugural Parson's Medal for Engineering Sciences by the Royal Irish Academy (RIA), in 2001. He was an elected to membership of the RIA, in 2004, served as a RIA Policy and International Relations Secretary from 2012 to 2016, and as the President, in 2017. He was the Vice-President for Region eight of the IEEE Circuits and Systems Society (CASS), from 2005 to 2007, a CASS Distinguished Lecturer, from 2012 to 2013, and the Chair of the CASS Distinguished Lecturer Program, in 2017. He served on the IEEE Fellows Committee and the IEEE Gustav Robert Kirchhoff Award Committee.

Elena Blokhina (S'05–M'06–SM'13) received the M.Sc. degree in physics and the Ph.D. degree in physical and mathematical sciences from Saratov State University, Russia, in 2002 and 2006, respectively, and the Habilitation (HDR) degree in electronic engineering from UPMC Sorbonne Universities, France, in 2017.

Since 2007, she has been with the School of Electrical and Electronic Engineering, University College Dublin, Ireland, where she is currently an Academic Staff Member and the Coordinator of the Circuits and Systems Research Group. Her research interests include the analysis, design, modeling, and simulations of nonlinear circuits, systems and networks with particular focus on complex, mixed-domain, and multi-physics systems.

Dr. Blokhina had been elected to serve as a member of the Boards of Governors of the IEEE Circuits and Systems Society, from 2013 to 2015, and has been a re-elected, from 2015 to 2017. She has served as a member of organizing committees, a review and programme committees, a session chair, and a track chair at many leading international conferences on circuits, systems, and electronics, including the IEEE International Symposium on Circuits and Systems (ISCAS), IEEE International Conference on Electronics, Circuits and Systems (ICECS), IEEE International Conference on Synthesis, Modeling, Analysis and Simulation Methods, and Applications to Circuit Design (SMACD) and others. She served as the Programme Co-Chair for the first edition of the IEEE Next Generation of Circuits and Systems Conference, in 2017 and of the 2018 edition of the IEEE International Conference on Electronics, Circuits and Systems. She is also the Chair of the IEEE Technical Committee on Nonlinear Circuits and Systems. She has served as a Guest Editor of the IEEE ACCESS and Springer *Analog Integrated Circuits and Signal Processing*, and as an Associate Editor for the IEEE TRANSACTIONS ON CIRCUITS AND SYSTEMS—I, where she is also the Deputy Editor-in-Chief.